BIOCHEMISTRY
including biophysical chemistry & molecular biology
Article

Biochemistry **2011,** *50,* 795–804 795
DOI: 10.1021/bi101286d

Loss of Membrane Targeting of Vangl Proteins Causes Neural Tube Defects†

Alexandra Iliescu,‡ Michel Gravel,‡ Cynthia Horth,‡ Zoha Kibar,§ and Philippe Gros*,‡

‡*Department of Biochemistry and Complex Traits Program, McGill University, Montreal, Canada H3G 0B1, and* §*Sainte-Justine Research Center, University of Montreal, Montreal, Canada H3T 1C5*

Received August 11, 2010; Revised Manuscript Received November 19, 2010

ABSTRACT: In the mouse, the *loop−tail* mutation (*Lp*) causes a very severe neural tube defect, which is caused by mutations in the *Vangl2* gene. In mammals, *Vangl1* and *Vangl2* code for integral membrane proteins that assemble into asymmetrically distributed membrane complexes that establish planar cell polarity in epithelial cells and that regulate convergent extension movements during embryogenesis. To date, *VANGL* are the only genes in which mutations cause neural tube defects in humans. Three independently arising *Lp* alleles have been described for Vangl2: D255E, S464N, and R259L. Here we report a common mechanism for both the naturally occurring *Lp* (S464N) and a novel ENU-induced mutation Lp^{m2Jus}(R259L). We show that the S464N and R259L variants stably expressed in polarized MDCK kidney cells fail to reach the plasma membrane, their site for biological function. The mutant variants are retained intracellularly in the endoplasmic reticulum, colocalizing with ER chaperone calreticulin. Furthermore, the mutants also show a dramatically reduced half-life of ∼3 h, compared to ∼22 h for the wild-type protein, and are rapidly degraded in a proteasome-dependent and MG132-sensitive fashion. Coexpressing individually the three known allelic *Lp* variants with the wild-type protein does not influence the localization of the WT at the plasma membrane, suggesting that the codominant nature of the *Lp* trait *in vivo* is due to haploid insufficiency caused by a partial loss of function in a gene dosage-dependent pathway, as opposed to a dominant negative phenotype. Our study provides a biochemical framework for the study of recently identified mutations in hVANGL1 and hVANGL2 in sporadic or familial cases of neural tube defects.

Neural tube defects (NTD)[1] are the second most common congenital malformations in humans affecting 1−2 infants per 1000 live births (*1*). In humans, the etiology of NTDs is poorly understood but is thought to involve interplay between complex genetic determinants and ill-defined environmental factors. This complexity has precluded the systematic identification of major gene effects associated with NTDs in humans. On the other hand, the study of naturally occurring or experimentally induced mouse mutants bearing NTDs (over 200 described to date) (*2*) has been a rich source of candidates whose relevance to the human condition can be readily tested in cohorts of sporadic or familial cases of NTDs (*3*−*5*). The loop−tail (*Lp*) mouse mutant is an established model for the study of NTDs in humans; *Lp*/+ heterozygote mice are viable but present a strongly kinked (looped) tail, while *Lp*/*Lp* homozygotes are not viable and suffer from a very severe NTD called craniorachischisis, characterized by a completely open neural tube, from the hindbrain to the most caudal region of the embryo (*6*−*8*).

We have previously shown that the NTD phenotype of *Lp* mice is caused by mutations in the *Vangl2* gene (*7*). *Vangl2* was originally identified in *Drosophila* as *Vang*/*Stbm* (Van Gogh/Strabismus), a so-called "core PCP gene", part of a group of genes that play a critical role in the establishment of planar cell polarity (PCP) of a number of structures in the fly (including the eye, the wing, and several cellular appendages) (*9*, *10*). Vang is an integral membrane protein that directly or indirectly interacts with other PCP proteins such as membrane-bound frizzled (Fz), diego (Dgo), flamingo (Fmi), cytoplasmic prickle (Pk), and disheveled (Dsh); the asymmetric distribution of the membrane-bound Dsh/Fz and Vang/Pk complex in epithelial cells is believed to propagate a polarity signal essential for PCP organization of cell layers (*11*). In the absence of Vang, Dsh and Pk are mislocalized, and PCP signaling is impaired (*12*). PCP genes and proteins have been highly conserved throughout evolution (*13*). In vertebrates, a clear example of PCP is the precise orientation of the stereocilliary bundles of the neurosensory epithelium of the organ of corti (inner ear) (*14*, *15*). Mouse mutants bearing mutations in vertebrate relatives of *Vang*/*Stbm* (*Vangl1*/*Vangl2*) (*16*, *17*), *Dsh* (*Dvl*) (*18*), and *Fmi* (*Celsr1*) (*19*) show disruption of these structures of the inner ear. In addition, vertebrate relatives of fly PCP genes regulate convergent extension (CE) movements during embryogenesis (*20*). CE movements contribute to several morphogenetic processes during embryogenesis, including the narrowing and lengthening of the neural plate critical to neural tube closure (*21*, *22*). The severe NTD phenotype (craniorachischisis) we originally described in *Vangl2* (*Lp*) (*6*, *7*) and *Vangl1*/*Vangl2* mutants (*16*) has since been reported for mutations in other mouse PCP genes such as *Dvl1*/*2* (*23*), *Dvl2*/*3* (*18*), *Celsr1* (*19*), and *Fz3*/*6* (*24*).

In mice and humans, there are two Vangl proteins, Vangl1 and Vangl2, that share over 80% sequence similarity. Both encode tetraspanning integral membrane proteins comprising of a PDZ-binding motif (PBM) in a large C-terminal intracytoplasmic tail

†This work was supported by a research grant to P.G. from the Canadian Institutes of Health Research (MOP-13425). P.G. is a James McGill Professor of Biochemistry.

*To whom correspondence should be addressed. Tel: 514-398-7291. Fax: 514-598-2603. E-mail: philippe.gros@mcgill.ca.

[1]Abbreviations: Lp, loop−tail; NTD, neural tube defects; PCP, planar cell polarity; CE, convergent extension; Fz, frizzled; Dgo, diego; Fmi, flamingo; Pk, prickle; Dvl, disheveled; PBM, PDZ-binding motif; PM, plasma membrane.

Published on Web 12/13/2010

that promotes interactions with PDZ-containing proteins (such as Dvl). Vangl1 and Vangl2 show a dynamic pattern of mRNA and protein expression during neural tube closure: Vangl1 is expressed primarily in ventral structures including the notochord, while Vangl2 is abundant on the dorsal side, with both expressed in the floor plate (*25*). Vangl1 and Vangl2 are also expressed in a number of additional tubular structures during embryogenesis (*25*). Partial inactivation of Vangl1/Vangl2 in double heterozygotes causes a NTD as severe as that seen in *Vangl2*$^{Lp/Lp}$ mutants, highlighting the critical role of both genes and proteins during neural tube formation and associated NTDs (*16*).

We have recently identified mutations in the human *VANGL1* gene in familial (V239I, R274Q) and sporadic cases (M328T) of neural tube defects (*3*, *4*). Some of these variants (V239I, M328T) were shown to abrogate interaction of VANGL proteins with DVL and impair convergent extension movements in a complementation assay in zebrafish (*3*, *26*). In addition, independent mutations in *VANGL2* (S84F, R353C, and F437S) have been identified in still-born human fetuses afflicted by severe NTDs (*5*); two of these mutations have been shown to abrogate (F437S) or significantly reduce (R353C) interaction of Vangl2 protein with members of the Dvl family. These results have identified VANGL1 and VANGL2 as critical genetic determinants in the etiology of NTDs in humans. Finally, we have identified three independent *Lp* alleles caused by independent mutations at *Vangl2*, namely, *Lp*^{m1Jus} (D255E) (*27*), *Lp* (S464N), and a novel *Lp*^{m2Jus} (R259L) (Kibar and Gros, unpublished), all of which map to the long cytoplasmic domain of Vangl2.

The biochemical mechanism of action of Vangl proteins in establishing PCP and mediating convergent extension movements during embryogenesis in vertebrates remains poorly understood. Likewise, the discrete molecular determinants required for assembly of membrane-bound Vangl-dependent signaling complexes and how such complexes may become nonfunctional in mice and humans bearing NTDs are unknown. Recently, we have established the biochemical characteristics of Vangl proteins in transfected MDCK cells and used several assays to identify the molecular basis for loss of function in the *Lp*^{m1Jus} *Vangl2* allele (D255E) (*27*). We have now characterized two additional *Lp*-associated loss-of-function variants, S464N (*Lp*) and R259L (*Lp*^{m2Jus}). The results show that, in all cases, loss of function is caused by impaired targeting of the protein to plasma membrane, which is associated with reduced half-life, and retention of the mutant variants in the endoplasmic reticulum.

EXPERIMENTAL PROCEDURES

Material and Antibodies. Cycloheximide was purchased from Sigma-Aldrich (St. Louis, MO). MG132 was from Calbiochem (San Diego, CA). Geneticin (G418), hygromycin, penicillin, and streptomycin were obtained from Invitrogen (Carlsbad, CA). All restriction enzymes were from New England Biolabs (Ipswich, MA). Taq DNA polymerase was from Invitrogen. The mouse monoclonal antibodies directed against the influenza hemagglutin epitope (HA.11) and the c-Myc epitope were purchased from Covance (Berkeley, CA). The mouse monoclonal antibody recognizing Na,K-ATPase (alpha) was from Santa Cruz Biotechnology (Santa Cruz, CA). The rabbit polyclonal antibody against calreticulin was obtained from Affinity BioReagents (Golden, CO). Cy3-conjugated goat anti-mouse and anti-rabbit antibodies and peroxidase-coupled goat anti-mouse antibody were from Jackson ImmunoResearch Laboratories (West Grove, PA). Alexa-Fluor 647-conjugated goat anti-mouse was from Invitrogen.

Plasmids and Constructs. The R259L and S464N mutations were introduced in the human *VANGL1* cDNA by PCR overlap extension mutagenesis, as described previously (*27*). The following nucleotides were used: 5′-ACCGATGGCGAGTCCCTCTTCTACAGCCTGGGACAC-3′ (forward Vangl1-R259L primer), 5′-GTGTCCCAGGCTGTAGAAGAGGGACTCGCCATCGGT-3′ (reverse Vangl1-R259L primer), 5′-CAGTGGAGGCTTGTCAATGATGAGGCTGTGACTAAT-3′ (forward Vangl1-S464N primer), and 5′-ATTAGTCACAGCCTCATCATTGACAAGCCTCCACTG-3′ (reverse Vangl1-S464N primer). Briefly, a short antigenic epitope (EQKLISEEDL) from the human c-Myc protein was introduced at the N-terminus of the *VANGL1* sequence. For quantification of protein cell surface expression, a hemagglutinin (HA) epitope (YPYDVPDYA) was inserted immediately after amino acid position 139 of each variant. To facilitate identification of transfected cells expressing recombinant proteins, c-Myc-tagged *VANGL1* was fused in-frame to the green fluorescent protein (GFP) by cloning into a modified peGFP-C1 vector (Clontech, Mountain View, CA). To study the effect of coexpression of wild type (WT) and mutant variants in the same cells, the c-Myc-tagged *VANGL1* cDNA without the HA epitope was fused to a fluorescent Cherry protein (from pmCherry; Clonetech), and the resulting Cherry fusion was subcloned into pcDNA3.1/Hygro(+) vector (Invitrogen) for expression in transfected cells.

Cell Culture and Transfection. Madin-Darby canine kidney (MDCK) epithelial cells were maintained in Dulbecco's modified Eagle's medium (DMEM) supplemented with 10% fetal bovine serum (FBS), 100 units/mL penicillin, and 100 μg/mL streptomycin at 37 °C in a 5% CO_2 incubator. For stable transfection, MDCK cells were transfected with cDNA constructs subcloned in peGFP-C1 using Lipofectamine Plus reagent (Invitrogen). Selection for stably transfected clones was in growth medium containing 0.3 mg/mL G418 for 10−14 days. Expression of recombinant GFP-VANGL1 R259L and S464N was initially identified by fluorescence microscopy on live cells and confirmed by Western blotting analysis of cell extracts. Total cell lysates were prepared in RIPA buffer (50 mM Tris-HCl, pH 7.5, 150 mM NaCl, 5 mM EDTA, 1% Triton X-100, 0.1% SDS supplemented with protease inhibitors), cleared by passage through a 25G needle and centrifugation at 13 000 rpm for 10 min (4 °C). Cell lysates (50 μg) were separated by electrophoresis using 7.5% SDS−polyacrylamide gels, followed by electroblotting and incubation with the monoclonal anti-c-Myc antibody 9E10 (used at 1:500). Immune complexes were revealed with a horseradish peroxidase conjugated goat anti-mouse antibody (1:10000) and visualized by enhanced chemiluminescence (SuperSignal West Pico kit, Thermo Scientific, Rockford, IL). For coexpression studies, stable MDCK cells expressing WT and D255E, R259L, or S464N variants were transfected as described above with Cherry-VANGL1 WT construct. Selection for stably transfected clones was in medium containing 0.3 mg/mL G418 and 0.3 mg/mL hygromycin for 10−14 days. Several clones coexpressing Cherry-VANGL1 WT and the GFP-VANGL1 variants were identified by fluorescence microscopy on live cells.

Crude Membrane Preparation. Crude membrane fractions from MDCK transfected cell clones were prepared as described (*27*). Cells were seeded in three 150 mm dishes and grown to confluency. After two washes in ice-cold phosphate-buffered saline (PBS) and once in cold NTE buffer (10 mM Tris-HCl, pH

7.5, 100 mM NaCl, 10 mM EDTA), cells were promptly harvested by scrapping in Tris-Mg buffer (10 mM Tris-HCl, pH 7.5, 1 mM $MgCl_2$ with proteinase inhibitors) followed by homogenization using a Dounce homogenizer. Unbroken cells and nuclei were removed by centrifugation (500*g* for 5 min), and a crude membrane fraction was prepared by centrifugation of the supernatant fraction at 50000*g* for 30 min. The final pellet containing the enriched membrane fraction was resuspended in NTE buffer supplemented with protease inhibitors.

Quantification of Cell Surface Expression by Enzyme-Linked Immunosorbent Assay. Quantification of cell surface expression of HA-tagged VANGL proteins in transfected MDCK cells was carried out by enzyme-linked immunosorbent assay as described previously (*28*) with the following modifications. MDCK cells stably expressing HA-tagged WT and R259L and S464N variants were seeded at near confluency in 24-well tissue culture plates and grown for 4 days. Cells were then washed with PBS and incubated in Ca^{2+}-free DMEM for 20 min, prior to incubation with 10 mM EGTA for 5 min. To evaluate the expression of HA-tagged proteins at the cell surface, cells were incubated with mouse anti-HA antibody (1:200 in Ca^{2+}-free DMEM) for 2 h at 37 °C/5% CO_2. Cells were washed, fixed with fresh 4% paraformaldehyde (PFA) in PBS for 15 min, and incubated with HRP-conjugated goat anti-mouse antibody (1:4000 in 5% skim milk) for 1 h. To evaluate the total amount of HA-tagged WT and mutant variants present, cells were fixed after the EGTA treatment, permeabilized with 0.1% Triton X-100 in PBS for 30 min, and blocked in 5% skim milk in PBS. Cells were then incubated with anti-HA antibody (1:200 in blocking solution) for 1 h, washed, and incubated with HRP-conjugated goat anti-mouse antibody (1:4000 in blocking solution). Peroxidase activity was quantified colorimetrically using the HRP substrate [0.4 mg/mL *O*-phenylenediamine dihydrochloride (OPD); Sigma-Aldrich] according to the manufacturer's instructions. After the cells were incubated for 30 min in the dark, the reaction was stopped using 50 μL of 3 M HCl per well containing 200 μL of reaction, and absorbance readings (490 nm) were taken in an ELISA plate reader. Background absorbance readings from nonspecific binding of primary antibody to vector-transfected cells were subtracted for each sample, and cell surface expression was normalized to total HA-tagged protein expression for each cell clone and was expressed as a percentage.

Pulse−Chase Assays and Determination of Relative Protein Stability. MDCK cells stably expressing WT, R259L, and S464N proteins were preincubated for 90 min at 37 °C in methionine- and cysteine-free DMEM medium containing 10% dialyzed FBS (labeling media). Thereafter, cells were pulse-labeled for 60 min at 37 °C with 2 mL of labeling medium containing 100 μCi of [^{35}S]methionine/cysteine (Perkin-Elmer, Boston, MA), as described previously (*27*). Cells were then washed twice with PBS and incubated in 2 mL of chase medium (DMEM containing 10% FBS, 15 μg/mL methionine, and 15 μg/mL cysteine), and incubation was continued for various times and up to 8 h. Cells were then lysed in 400 μL of RIPA buffer. For immunoprecipitation, equal amounts of cell lysates (adjusted to 1 mg/mL in RIPA buffer) were incubated with the mouse anti-Myc antibody 9E10 (2.5 μg) overnight at 4 °C, followed by incubation with protein A/G−Sepharose (GE Healthcare, Piscataway, NJ) for 4 h. Beads were washed three times in RIPA buffer, and proteins were eluted with 50 μL of 2× sample buffer. The radiolabeled proteins were separated by electrophoresis using 7.5% SDS−polyacrylamide gels. The gels were then fixed, impregnated with Amplify (GE Healthcare, Piscataway, NJ), dried, and exposed to film. Densitometric analysis was performed by using NIH ImageJ software (NIH, Bethesda, MD). In certain experiments aiming to measure protein stability, MDCK cells expressing WT and R259L and S464N variants were treated with cycloheximide (20 μg/mL) for 4 h to inhibit protein synthesis. When used, the proteasome inhibitor MG132 (5 μg/mL) and chloroquine (100 μM) were added to the growth media supplemented with cycloheximide. Cells treated in this manner were lysed with RIPA buffer, and protein stability was monitored by Western blotting.

Immunofluorescence and Confocal Microscopy. For subcellular localization studies, MDCK cells stably expressing WT or mutant variants were seeded at high density onto glass coverslips in a 24-well plate. Twenty-four hours later, cells were washed twice with ice-cold PBS, fixed for 15−20 min in 4% PFA in PBS, and then permeabilized using 0.5% Triton X-100 in PBS for 15 min (permeabilized conditions). Cells were blocked with 5% goat serum in PBS for 1 h, followed by incubation with primary antibody [mouse anti-Na,K-ATPase (1:50); mouse anti-HA (1:200); rabbit anti-calreticulin (1:100)] for 1 h and washing three times with 0.1% BSA in PBS. Finally, the coverslips were incubated for 1 h with the appropriate secondary antibody [goat anti-mouse Cy3 (1:1000); goat anti-rabbit Cy3 (1:1000); Alexa-Fluor 647-conjugated goat anti-mouse (1:1000)] and washed three times with PBS. All of the incubations were done at room temperature, and the antibodies were all diluted in blocking solution. To detect cell surface expression of the exofacial HA epitope engineered in VANGL proteins (nonpermeabilized conditions), MDCK cells expressing HA-tagged WT and R259L and S464N variants were incubated with the mouse anti-HA (1:200) in DMEM containing 2% nonfat milk for 2 h at 37 °C. After several washes with PBS, cells were fixed for 15 min with 4% PFA in PBS and incubated with goat anti-mouse Cy3 antibody (1:1000) for 1 h. For immunofluorescence, coverslips were rinsed once in water and mounted using Permafluor aqueous mounting medium (Thermo Scientific, Fremont, CA). Confocal microscopy was performed using a Zeiss LSM5 Pascal laser scanning confocal microscope. All image analyses were performed using the LSM5 Image software. To maximize image quality, a Median filter 3 × 3 was applied to the images using Image-Pro software. To remove out-of-focus fluorescence, the Z stack sections were also deconvoluted using 10 iterations with AutoQuant software.

RESULTS

Expression and Subcellular Localization of WT and R259L and S464N Variants in MDCK Cells. The *Lp*-associated D255E, R259L, and S464N mutations affect highly conserved residues in the large intracellular cytoplasmic segment of Vangl proteins (Figure 1). In addition, the R259L mutation maps close to the mouse D255E (Lp^{m1Jus} allele) (*27*) and the V239I *de novo* loss-of-function *VANGL1* mutation detected in a human case of familial NTD (*3*), suggesting that this protein segment is critical for a yet to be defined aspect of VANGL protein structure and function. To investigate the effect of the R259L and S464N mutations on the biochemical properties of VANGL proteins, the two variants were expressed as GFP fusion proteins in MDCK cells. This cell type was chosen since it is derived from a lineage that normally expresses VANGL proteins *in vivo* during kidney tubulogenesis (*25*) and is therefore likely to possess the cellular machinery required for proper expression,

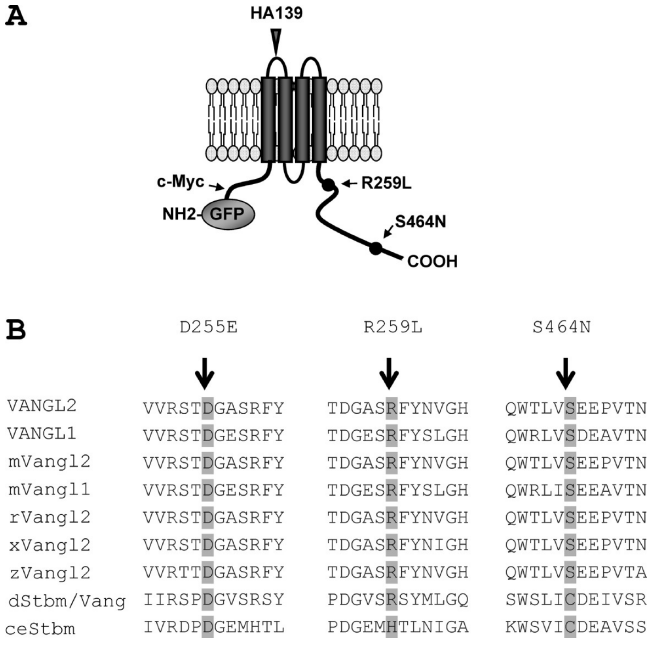

FIGURE 1: Schematic representation of the GFP-Vangl1 protein. (A) The positions of the hemagglutin (HA) tag inserted at position 139 (predicted TM1-TM2 connecting loop), the c-Myc tag inserted in the amino-terminal segment, the GFP fused at the N-terminus, and the R259L and S464N mutations in the intracellular C-terminal region are shown. (B) Sequence conservation across species of the R259 and S464 amino acids mutated in *Lp* mice.

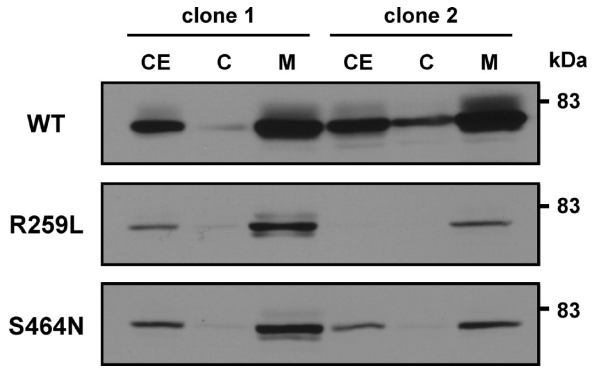

FIGURE 2: Expression of WT and R259L and S464N Vangl1 variants in the membrane fraction of transfected MDCK cells. Independent MDCK cell clones stably expressing either wild type (WT) or R259L and S464N mutant variants were isolated. Total cell extracts (CE), membrane-enriched fractions (M), and soluble cytoplasmic extracts (C) were prepared from these cells, and equal amounts of protein (50 μg) were analyzed by Western blotting analysis with the mouse monoclonal antibody 9E10 directed against the c-Myc tag inserted in-frame near the amino terminus of the recombinant proteins.

maturation, membrane insertion, and subcellular targeting of the protein.

Several transfected MDCK cell clones stably expressing either WT or R259L and S464N variants were initially identified by GFP fluorescence, and recombinant protein expression was confirmed by Western blot analysis (Figure 2) of total cell extracts and crude membrane fractions from independent MDCK clones. In these cells, the protein was expressed as a specific HA-immunoreactive species of ~80 kDa present in total cell extracts and greatly enriched in crude membrane extracts from individual MDCK clones tested, suggesting that the R259L and S464N mutations do not impair membrane association of the

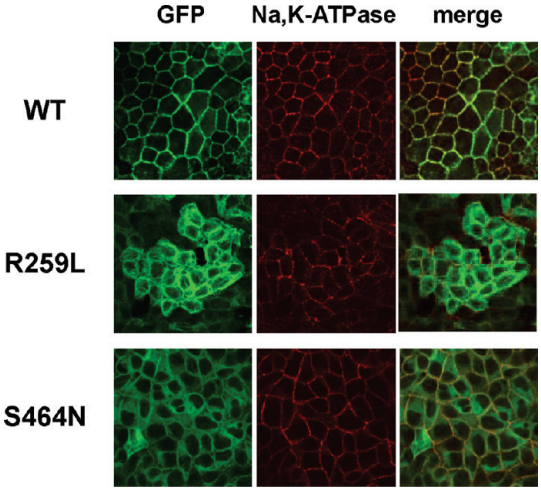

FIGURE 3: Cellular localization of WT and R259L and S464N Vangl1 variants in transfected MDCK cells. Transfected MDCK cells stably expressing GFP-Vangl1 WT, R259L, and S464N (green) were grown to confluence, fixed, permeabilized and stained for Na,K-ATPase followed by Cy3-conjugated secondary antibody (red), and examined by confocal microscopy. The merge images show that while the majority of WT signal is associated to the plasma membrane and overlaps with Na,K-ATPase (yellow), the R259L and S464N staining is mostly intracellular. Images are representative of at least three independent experiments of each type.

protein. However, in multiple independent transfected clones analyzed, we noted a lower overall expression level of the R259L and S464N variants compared to WT (Figure 2; data not shown). A possible effect of the R259L and S464N mutations on subcellular distribution and plasma membrane (PM) targeting was next investigated by immunofluorescence and confocal microscopy (Figure 3). MDCK transfectants expressing the WT protein displayed a strong PM localization (Figure 3, top panels), producing a typical mesh-like signal in confluent monolayers and showing colocalization with Na,K-ATPase, a specific marker for basolateral membrane of MDCK cells (Figure 3, top center panel). By contrast, R259L and S464N signals did not appear concentrated at the PM but rather showed an intracellular punctate pattern suggestive of localization to an intracellular endomembrane compartment (Figure 3, middle and bottom panels). In addition, R259L and S464N did not colocalize with the PM marker Na,K-ATPase. The seemingly distinct subcellular localization of the WT and *Lp*-associated variant proteins was confirmed by examination of cell sections (Z stacks) (Figure 4). Indeed, while the WT protein was expressed predominantly at the basal and lateral membranes of polarized MDCK cells (Figure 4, left panels), colocalizing with Na,K-ATPase (Figure 3, left middle panel), R259L and S464N were not present at the basolateral membrane but were found in an intracellular compartment negative for Na,K-ATPase (Figure 4, center and right panels). Together, these results strongly suggest that the pathogenic, *Lp*-associated mutations, R259L and S464N mutations, interfere with normal subcellular targeting of the protein.

Surface Expression of WT and R259L and S464N Variants in MDCK Cells. We previously used immunofluorescence with an exofacial HA epitope (inserted at position 139 in the extracellular loop delineated by TM1-TM2 segments; see Figure 1A) to demonstrate cell surface expression of WT VANGL1 protein (*27*). To further investigate a possible effect of the R259L and S464N mutations on PM targeting, we similarly monitored cell surface expression of these two variants

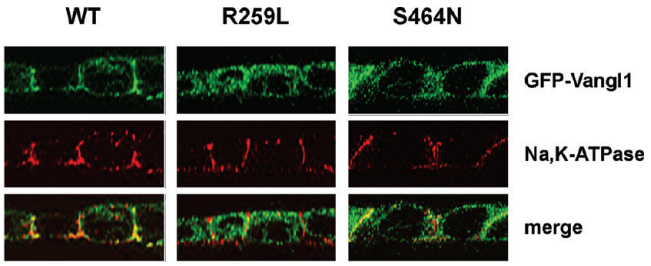

FIGURE 4: Subcellular localization of the WT and R259L and S464N Vangl1 variants in stably transfected MDCK cells: Z-line image analysis. Transfected MDCK cells stably expressing either GFP-Vangl1 WT, R259L, or S464N mutant variants were processed as described in the legend to Figure 3. Cells were analyzed by confocal microscopy to visualize the expression of GFP-Vangl1 (green) and Na,K-ATPase (red). Representative X−Z sections are shown. The merge images show that while GFP-Vangl1 WT colocalizes with Na, K-ATPase at the basolateral membrane (yellow) of the polarized cells,the R259L and S464N mutants are absent at that site and are mainly localized to an intracellular compartment.

in confluent MDCK cells. The polarity of the HA tag with respect to PM was determined by immunofluorescence with an anti-HA antibody used in intact cells (extracellular) and in cells permeabilized with Triton X-100 (intracellular) (Figure 5) (*27*). A strong fluorescence signal was detected in both permeabilized and nonpermeabilized MDCK clones expressing the WT protein (Figure 5A, left panels); this signal was absent from control untransfected MDCK cells similarly exposed to the anti-HA antibody (data not shown). By contrast, MDCK clones expressing the R259L and S464N variants displayed bright intracellular fluorescence under permeabilization conditions (Figure 5A, top center/right panels) but showed no fluorescence under nonpermeabilized conditions (Figure 5A, bottom center/right panels), suggesting that R259L and S464N are not expressed at the PM. The presence/absence of a immunoreactive HA tag at the surface of cells expressing WT, R259L, and S464N proteins was also investigated by an ELISA-based assay (*28*). For this, corresponding MDCK transfectants were incubated with anti-HA antibody with or without prior permeabilization. The amount of bound anti-HA antibody was quantified using a secondary antibody coupled to horseradish peroxidase. Results show that while 78 ± 6% of total immunoreactive WT protein was found at the cell surface (Figure 5B), only a modest fraction of R259L (35% ± 6%) and S464N (29% ± 4%) was detected at that site. Together, results in Figures 3−5 show that the two *Lp*-associated mutations, R259L and S464N, disrupt normal subcellular localization and interfere with normal PM targeting.

Stability of the R259L and S464N Variants in MDCK Cells. The overall lower level of the R259L and S464N variants detected in transfected MDCK cells (compared to WT; Figure 2 and data not shown), together with the noted defect in subcellular targeting of the variant, prompted us to analyze a possible effect of the mutations on protein half-life and stability as measured by pulse−chase experiments. MDCK clones expressing WT and R259L and S464N variants were labeled with [^{35}S]methione/cysteine for 60 min (pulse), and the fate of the radiolabeled proteins was followed for 8 h by immunoprecipitation using extracts from pulsed cells grown in isotope-free medium (chase). Representative autoradiograms and quantification from four independent experiments are shown in panels A and B of Figure 6, respectively. In these experiments, the half-life of WT protein in MDCK cells was estimated at greater than 20 h, while the half-lives of R259L and S464N were found to be shorter than ~3 h.

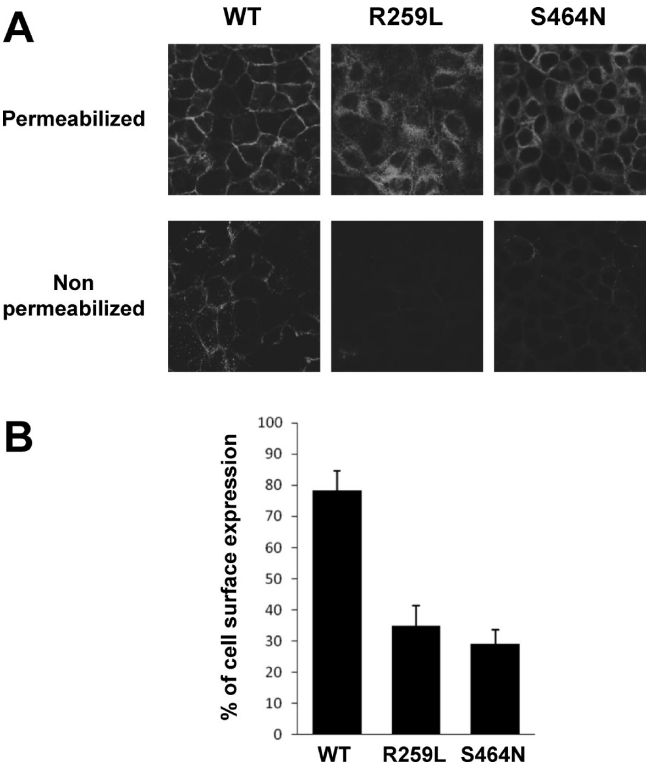

FIGURE 5: Analysis of plasma membrane targeting and surface expression of WT and R259L and S464N Vangl1 variants in MDCK cells. (A) MDCK cells stably expressing HA-tagged GFP-Vangl1 WT, R259L, and S464N were analyzed by immunofluorescence to detect surface expression of an HA antigenic epitope inserted at position 139 in the predicted TM1-TM2 connecting loop. Immunofluorescence was carried out either on intact cells (nonpermeabilized) or in cells pretreated with 0.1% Triton X-100 (permeabilized), using a mouse anti-HA antibody. Cells were incubated with Cy3-conjugated secondary antibody, and images were acquired by confocal microscopy. Images are representative of at least five independent experiments of each type. (B) In other experiments, the same cells exposed to the anti-HA antibody were incubated with an HRP-coupled secondary anti-mouse antibody, and the amount of the primary antibody bound was determined for both conditions (permeabilized and nonpermeabilized) by a colorimetric reaction using an HRP substrate quantitated by spectrometry. The amount of HA-tagged WT, R259L, and S464N proteins expressed at the cell surface (detected in nonpermeabilized cells) is shown as a fraction (%) of total protein expression (measured in permeabilized cells).

Results from the pulse−chase experiments strongly suggest that both R259L and S464N mutations cause a strong decrease in protein stability.

Retention of the R259L and S464N Variants in the Endoplasmic Reticulum. The reduced half-life, the absence of PM targeting, and the localization of the R259L and S464N variants to a subcellular endomembrane compartment suggested that they may have a defect in maturation associated with retention of the protein in the endoplasmic reticulum (ER). This possibility was tested by immunofluorescence using an antibody directed against the ER marker calreticulin. Results show that while the WT protein displayed no colocalization with the intracellular punctate ER staining produced by calreticulin (Figure 7, top panels), there was significant colocalization of R259L and S464N and calreticulin, suggesting that both variants are present in the ER endomembrane compartment (Figure 7, middle and bottom panels).

Retention of inappropriately folded proteins in the ER, including membrane proteins, ultimately leads to degradation

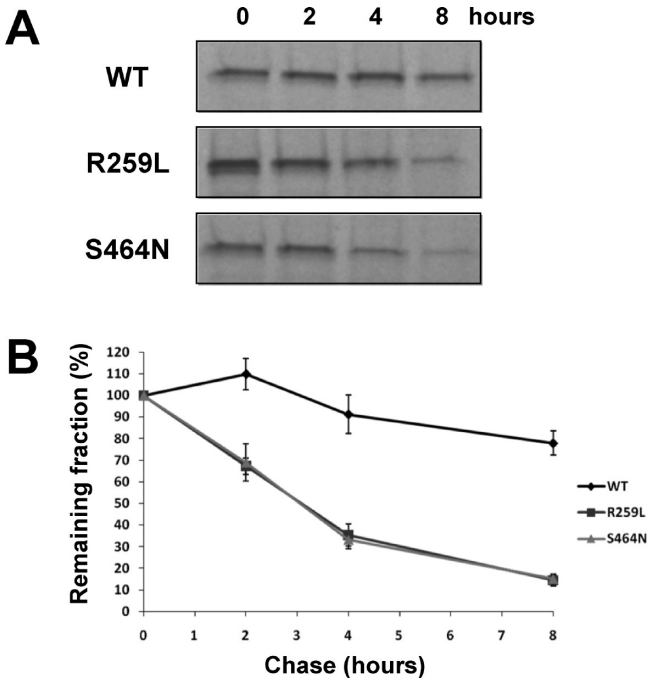

FIGURE 6: Pulse–chase studies of GFP-Vangl1 WT, R259L, and S464N proteins expressed in MDCK cells. (A) MDCK cells stably expressing GFP-Vangl1 WT, R259L, or S464N were metabolically labeled by a 60 min pulse of ^{35}S-Met/Cys. The cells were transferred to radioactivity-free medium, followed by different chase periods. Cell lysates were prepared and subjected to immunoprecipitation followed by gel electrophoresis and autoradiography. To obtain comparable signal intensity at T0, the R259L and S464N blots were exposed for longer times. (B) Estimation of the rate of disappearance of WT, R259L, and S464N labeled proteins. The amount of radiolabeled WT, R259L, and S464N proteins was quantified (pixel density of each band) from scanning the autoradiograms and expressed as a fraction (%) of the sample at T0, which is set at 100%. The graph represents the mean of four experiments ± SE.

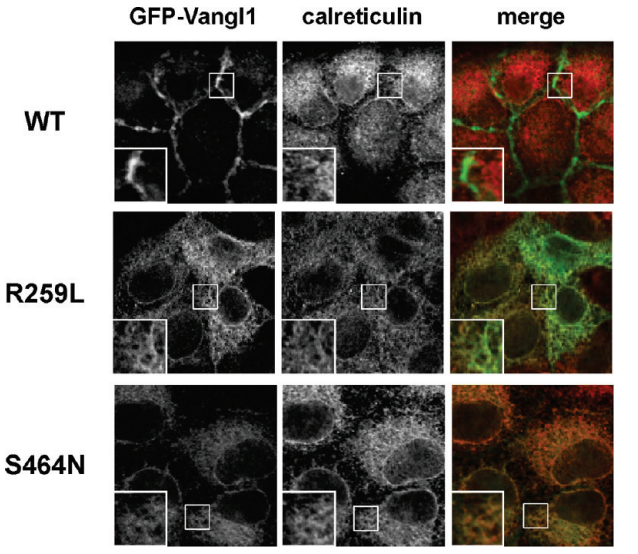

FIGURE 7: Determination of subcellular localization of R259L and S464N variants by double immunofluorescence. MDCK cells stably expressing WT, R259L, or S464N were fixed and immunostained for the endoplasmic reticulum marker calreticulin (red). As opposed to GFP-Vangl1 WT, which is expressed at the plasma membrane, the R259L and S464N mutants show intracellular staining that significantly overlaps with calreticulin. Insets are magnifications of the indicated areas.

via the proteasome (*29*). To analyze the behavior of the R259L or S464N variants with respect to proteasome-mediated degradation, MDCK clones expressing the corresponding proteins were exposed to cycloheximide (CHX) in either the presence or absence of the proteasome inhibitor MG132 (Figure 8). Cell extracts were prepared and analyzed by immunoblotting (Figure 8A), and the signal was quantified (Figure 8B). CHX treatment of WT, R259L, and S464N expressing cells had a differential effect on the level of protein remaining after 4 h of treatment, with an ~80% decrease in R259L and S464N variants, compared to only a small reduction in the amount of WT protein. Addition of the proteasome inhibitor MG132 to cells treated with CHX resulted in a dramatic increase in the amount of detectable R259L and S464N variants (~70% of untreated controls) in these cell extracts. MG132/CHX treatment also resulted in a modest increase of detectable WT protein (when compared to CHX treatment alone). Furthermore, the addition of chloroquine, a lysosome inhibitor, did not prevent the rapid degradation of both R259L and S464N (Figure 8). Together, these results suggest that R259L and S464N proteins are retained in the ER, where they are targeted for degradation in a proteasome-dependent manner.

Coexpression and Cellular Localization of Vangl WT and Mutant Proteins in MDCK Cells. For the D255E and S464N variants, heterozygote mice exhibit a mild looped-tail phenotype, whereas homozygotes exhibit both looped tail and craniorachischisis (*6*, *7*). This codominance phenotype is the same for both D255E and S464N variants, while the phenotype of R259L appears somewhat less severe (*6*, *7*) (Kibar and Gros, unpublished). Codominance could be explained by (a) a partial or complete loss of function of the mutant gene/protein in a gene dosage pathway (haploid insufficiency) or (b) a gain of function (dominant negative effect) in which the mutant protein interferes with the normal maturation/targeting of the WT protein produced in the same cell. Arguments favoring haploid insufficiency (*16*) and dominant negative effects (*30*) to explain the codominance inheritance of *Lp* have been published. To study the effect of the three known *Lp*-associated variants, D255E, R259L, and S464N, on targeting of the WT and protein and vice versa, a Cherry-WT protein was stably coexpressed in independent MDCK cell clones expressing either WT, D255E, R259L, and S464N (all fused to GFP). Several stably double-transfected MDCK clones were identified by fluorescence, and Cherry-VANGL 1 and GFP-VANGL1 protein coexpression was confirmed by immunoblotting (Supporting Information Figure S1) and fluorescence-activated cell sorting (data not shown). These experiments also indicated similar levels of coexpression of the Cherry and GFP-tagged proteins in the cell clones analyzed by microscopy. The cellular localization of Cherry- and various GFP-tagged proteins (WT, D255E, R259L, and S464N) in MDCK cells was analyzed by confocal microscopy (Figure 9 and Supporting Information Figure S2). As expected, the coexpressed Cherry- and GFP-tagged WT proteins were both found at the PM, where they colocalized with the Na,K-ATPase PM marker. Coexpression in the same cells of Cherry-WT with either D255E, R259L, or S464N (GFP-tagged) did not affect the PM staining of the Cherry-WT protein. In each case, the GFP-tagged D255E, R259L, and S464N proteins displayed mostly an ER-like staining, while the Cherry-WT colocalized with Na,K-ATPase marker, suggesting that expression of the mutant variant did not affect maturation and PM targeting of the WT protein. Expression of the various mutant variants of VANGL1 also did not affect the distribution and subcellular localization of WT

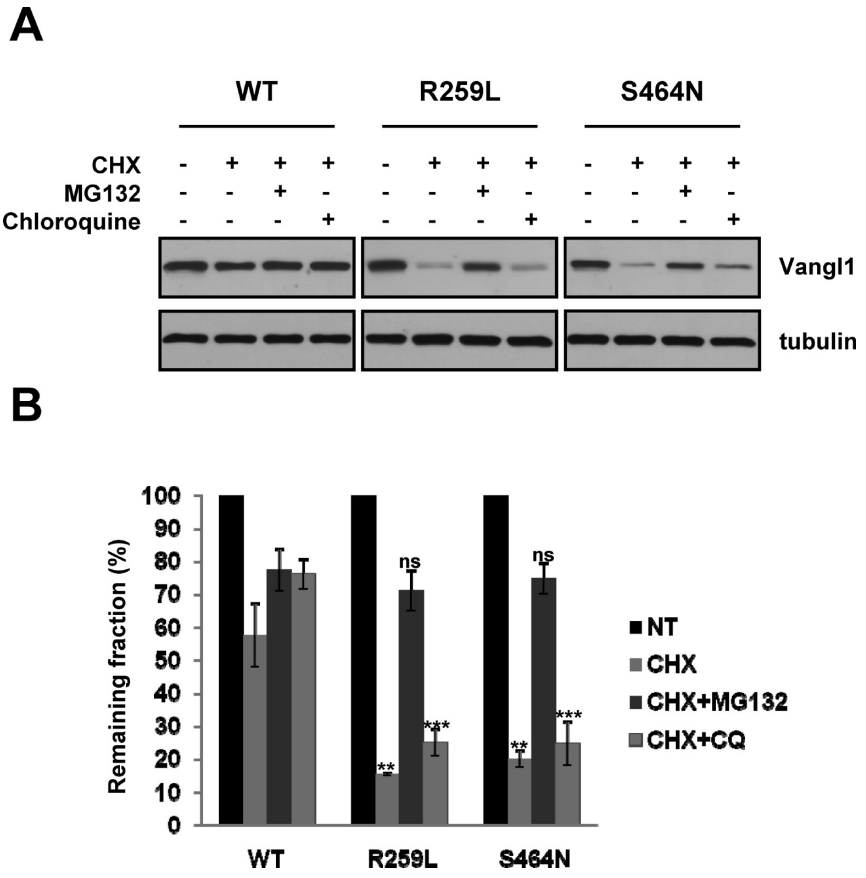

FIGURE 8: Cellular degradation of WT and R259L and S464N Vangl1 variants in MDCK cells. (A) Stably transfected MDCK cells expressing either GFP-Vangl1 WT, R259L, or S464N were grown to confluence and treated with cycloheximide (20 μg/mL) for 4 h, in either the absence or presence of the proteasome inhibitor MG132 (5 μg/mL) or the lysosome inhibitor chloroquine (100 μM). Cell lysates (50 μg) were subjected to gel electrophoresis and Western blot analysis using the anti-c-Myc antibody. Tubulin was used as an internal loading control and was detected using a mouse monoclonal antiserum. The rapid degradation of R259L or S464N variants was prevented by MG132, but not by chloroquine, indicating that the R259L and S464N proteins are mainly degraded by the proteasome. To obtain comparable signal intensity, the R259L and S464N blots were exposed for longer times than those containing WT protein. (B) The effect of MG132 and chloroquine on the stability of WT and R259L and S464N mutant proteins after 4 h of treatment was quantitated by densitometry scanning as described in the legend of Figure 6. Each value represents mean ± SE of four independent experiments. Statistical significance of intergroup difference was determined by Student's *t* test, where ** and *** were found to be significant ($P < 0.01$ and ($P < 0.001$, respectively); NS, not significant.

VANGL1 (fused to Cherry), as determined by Z stack analysis (Supporting Information Figure S2) and surface biotinylation (data not shown). These results support the contention that D255E, R259L, and S464N mutations represent a loss of function of the mutated protein in a gene dosage-dependent pathway (haploid insufficiency) and argue against a dominant negative effect of the three mutations.

DISCUSSION

Vangl proteins are integral membrane proteins that play a critical role in two pathways that control cell and tissue morphogenesis during development: planar cell polarity (PCP) and convergent extension movements (CE) (*13*, *17*). Although the precise mechanism of action of Vangl proteins in PCP and CE in vertebrates remains elusive, independent mutations in *Vangl* genes have been associated with neural tube defects in mice and humans (*3*−*7*). In mice, homozygote mutations in *Vangl2* (*Lp*) (*6*, *7*) and double heterozygosity for loss of function mutations at *Vangl1* and *Vangl2* (*16*) cause craniorachischisis. In the mouse, there are three independent *Lp* alleles at *Vangl2*, the spontaneously arising S464N (*Lp*)(*7*) and two chemically induced D255E (Lp^{m1Jus}) (*6*) and R259L (Lp^{m2Jus}) (Kibar and Gros, unpublished). Herein, we have studied the molecular basis of the loss-of-function variants S464N and R259L, after expression of these proteins in polarized MDCK kidney epithelial cells. In our study, human *VANGL1* was used as a molecular backbone. Although the pathogenic R259L and S464N mutations emerged in *VANGL2*, much data indicate that VANGL1 and VANGL2 proteins are functionally equivalent (*16*, *26*, *31*). Thus, the choice of the molecular backbone should not impact the biochemical characterization of pathogenic mutations, as we reported previously (*27*).

We found that both mutations impaired plasma membrane targeting and surface expression of the protein (absence of colocalization with Na,K-ATPase), with both mutant variants being retained in the calreticulin-positive endoplasmic reticulum. The S464N and R259L proteins also show a dramatic reduction in half-life (from 22 h for the WT protein to 3 h for both mutants) and stability in MDCK, with increased degradation by a proteasome-dependent and MG132-sensitive fashion. These characteristics are similar to those we previously reported for the D255E *Lp*-allele (*27*) and suggest a common mechanism for the loss of function of the three pathogenic *Lp*-associated variants, namely, absence of expression of the protein at the plasma membrane. The mutations appear to cause a maturation defect with retention of the mutant variants in the ER. Our findings are in agreement with the previous demonstration that PCP signaling requires membrane targeting and asymmetric distribution of complexes containing Vangl proteins.

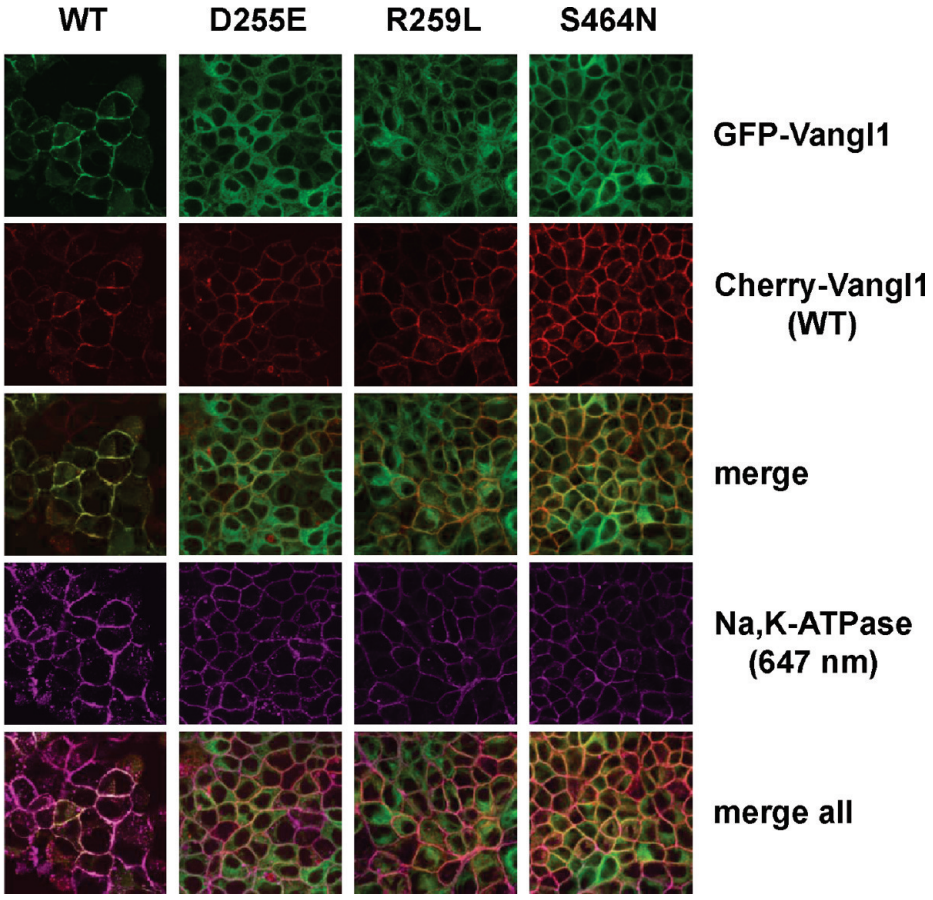

FIGURE 9: Coexpression and cellular localization of WT and Lp-associated variants (D255E, R259L, and S464N) in MDCK cells. Stably transfected MDCK cells coexpressing Cherry-Vangl1 WT (red) with either GFP-tagged (green) WT, R259L, S464N, or D255E were grown to confluency, fixed, permeabilized and stained for Na,K-ATPase followed by Alexa-Fluor 647-conjugated secondary antibody (violet), and examined by confocal microscopy. The merged images show that while the majority of GFP-Vangl1 WT signal is associated to the plasma membrane and overlaps with Cherry-Vangl1 WT (yellow), the GFP-tagged D255E, R259L, and S464N staining is mostly intracellular and does not influence the staining for Cherry-Vangl1 which remains associated to the plasma membrane. Images are representative of at least three independent experiments of each type with two different clones.

Our combined analysis of the *Lp*-associated *Vangl2* variants D255E, S464N, and R259L also point to a critical structural/functional role of the large predicted intracytoplasmic domain of the protein, as all three mutations map within this segment (*32*). Likewise, the three *VANGL1* variants (V239I, R274Q, and M328T) we detected in the heterozygote state in sporadic and familial cases of neural tube defects in humans also map to the cytoplasmic domain of the protein (*3*). Finally, two mutations in this portion of the *VANGL2* protein (R353C and F437S) were recently identified in fetuses bearing severe neural tube defects (*5*). Although the clustering of pathogenic mutations in this part of the protein clearly suggests a critical role for this segment, the variable nature of the mutations being either subtle (V239I, D255E, S464N) or nonconservative (R259L, R353C), together with the absence of any obvious structural/functional motifs or signatures being interrupted by these variants, does not suggest an obvious mechanistic basis for the mutation effects. The C-terminal domain is highly conserved between the different members of the Vangl/Stbm family (e.g., 72% sequence identity and 85% sequence conservation between mouse and fish Vang1), and several residues affected by mutations are either invariant (V239, D255, F437) or highly conserved (R259, R274, M328, R353, S464) in the Vangl protein family. One of the mutations, R274Q, alters a key residue in a D-box consensus sequence of ubiquitination (RXXLXXXXE/N/D); however, this motif is not preserved beyond the mouse and human Vangl1 sequence, and its relevance to a conserved mechanism of action of Vangl proteins remains unknown. On the other hand, Vangl proteins have recently been suggested to interact with sec24b, a cargo sorting member of COPII vesicle (*33*). COPII complex is part of the ER to Golgi transport, implicated in selectively trafficking Vangl2. In addition, studies in mice with either inactive (ENU-induced) or knockout alleles at *sec24b* display craniorachischisis, CE and PCP defects (*34*). It was also additionally demonstrated that the two *Lp*-associated mutations D255E and S464N fail to sort into COPII vesicles and remain trapped in the ER (*33*). These observations are compatible with the biochemical properties, including lack of PM association, reduced half-life, and retention in the ER of the three *Lp* mutations we present in the current study. Although retention of inappropriately folded proteins in the ER may induce the UPR (unfolded protein response) in which the expression of ER-resident chaperones (calnexin, BIP, PDI) is unregulated, we note that expression of the R259L and S464N variants fails to induce the UPR in MDCK cells (data not shown).

In vivo, two *Lp* mutations, D255E and S464N, are inherited in a codominant fashion with heterozygotes showing the mild looped-tail phenotype, while *Lp*/*Lp* homozygotes show the very severe craniorachischisis and die *in utero*. The codominance characteristics of *Lp* can be explained by haploid insufficiency

caused by a partial loss of function in a gene dosage-dependent pathway; alternatively, it may result from a negative dominance caused by a gain of function of the mutant variant which alters the activity of the normal protein encoded by the intact wild-type allele present in the heterozygotes. The observation that two allelic variants (D255E, S464N) at *Lp* (a) display exactly the same phenotype in the heterozygote state *in vivo* and (b) are associated with impaired maturation/processing and absence of membrane expression *in vitro* strongly suggest that these mutations cause a loss of function in a gene dosage-dependent pathway. Nevertheless, others have recently suggested that *Lp* alleles behave as dominant negative (*30*), with the mutant variant altering normal maturing, processing, targeting, or function of the a coexpressed wild-type protein. Results shown in Figure 9 show that coexpression of individual *Lp* mutants with the wild-type protein in MDCK cells (mimicking the situation of *Lp*/+ heterozygotes) fails to influence the subcellular localization and PM targeting of the wild-type protein. These results do not support a dominant negative effect of *Lp* mutations and favor a loss-of-function mechanism. However, we cannot formally exclude the possibility that mutant VANGL variants might sequester (or liberate, and hence mistarget) a different but essential interaction partner present in limiting quantities. On the other hand, the R259L variant shows a low frequency of "looped-tail" animals in heterozygotes, while R259L homozygotes display very severe craniorachischisis (Kibar and Gros, unpublished). The reduced frequency of "looped-tail" animals in R259L/+ heterozygotes may suggest that R259L is less detrimental to protein function *in vivo* (as suggested by reduced but not abrogated surface expression of this mutant). It may also be caused by possible genetic background effects (in the original ENU mutagenized mouse stock) that modulate penetrance or expressivity of an otherwise loss-of-function variant.

In conclusion, our results suggest that Vangl proteins are part of a very sensitive gene dosage-dependent pathway during the development of the neural tube and that *Lp* alleles (D255E, R259L, S464N) behave as loss-of function mutations. Furthermore, we show that both the S464N and the novel *Lp* alleles R259L are unable to reach the plasma membrane, potentially affecting the delicate balance in the PCP pathway and leading to NTDs. Taken together, our biochemical analyses, of mutant *Lp* variants in MDCK cells provide an experimental framework for the future analysis of *h*VANGL1/*h*VANGL2 mutations detected in familial and sporadic cases of NTDs.

ACKNOWLEDGMENT

Image acquisition, data analysis, and image processing were done on equipment and with the assistance of the McGill Life Science Complex Imaging Facility which is founded by the Canadian Foundation for Innovation. We also thank Nassima Fodil-Cornu, Ajitha Thanabalasuriar, and Irena Radovanovic for their help and technical advice.

SUPPORTING INFORMATION AVAILABLE

Western blot analysis of the expression of Cherry-VANGL1 WT protein in MDCK cells stably coexpressing GFP-VANGL1 WT, D255E, R259L, or S464N proteins and Z-line image analysis of subcellular localization of Cherry-VANGL1 WT protein in MDCK cells stably coexpressing GFP-VANGL1 variants. This material is available free of charge via the Internet at http://pubs.acs.org.

REFERENCES

1. Copp, A. J., and Greene, N. D. (2010) Genetics and development of neural tube defects. *J. Pathol. 220*, 217–230.
2. Bassuk, A. G., and Kibar, Z. (2009) Genetic basis of neural tube defects. *Semin. Pediatr. Neurol. 16*, 101–110.
3. Kibar, Z., Torban, E., McDearmid, J. R., Reynolds, A., Berghout, J., Mathieu, M., Kirillova, I., De Marco, P., Merello, E., Hayes, J. M., Wallingford, J. B., Drapeau, P., Capra, V., and Gros, P. (2007) Mutations in VANGL1 associated with neural-tube defects. *N. Engl. J. Med. 356*, 1432–1437.
4. Kibar, Z., Bosoi, C. M., Kooistra, M., Salem, S., Finnell, R. H., De Marco, P., Merello, E., Bassuk, A. G., Capra, V., and Gros, P. (2009) Novel mutations in VANGL1 in neural tube defects. *Hum. Mutat. 30*, E706–E715.
5. Lei, Y. P., Zhang, T., Li, H., Wu, B. L., Jin, L., and Wang, H. Y. (2010) VANGL2 mutations in human cranial neural-tube defects. *N. Engl. J. Med. 362*, 2232–2235.
6. Kibar, Z., Underhill, D. A., Canonne-Hergaux, F., Gauthier, S., Justice, M. J., and Gros, P. (2001) Identification of a new chemically induced allele (Lp(m1Jus)) at the loop-tail locus: morphology, histology, and genetic mapping. *Genomics 72*, 331–337.
7. Kibar, Z., Vogan, K. J., Groulx, N., Justice, M. J., Underhill, D. A., and Gros, P. (2001) Ltap, a mammalian homolog of *Drosophila* Strabismus/Van Gogh, is altered in the mouse neural tube mutant loop-tail. *Nat. Genet. 28*, 251–255.
8. Murdoch, J. N., Doudney, K., Paternotte, C., Copp, A. J., and Stanier, P. (2001) Severe neural tube defects in the loop-tail mouse result from mutation of Lpp1, a novel gene involved in floor plate specification. *Hum. Mol. Genet. 10*, 2593–2601.
9. Goodrich, L. V. (2008) The plane facts of PCP in the CNS. *Neuron 60*, 9–16.
10. Roszko, I., Sawada, A., and Solnica-Krezel, L. (2009) Regulation of convergence and extension movements during vertebrate gastrulation by the Wnt/PCP pathway. *Semin. Cell Dev. Biol. 20*, 986–997.
11. Strutt, H., and Strutt, D. (2009) Asymmetric localisation of planar polarity proteins: mechanisms and consequences. *Semin. Cell Dev. Biol. 20*, 957–963.
12. Bastock, R., Strutt, H., and Strutt, D. (2003) Strabismus is asymmetrically localised and binds to prickle and dishevelled during *Drosophila* planar polarity patterning. *Development 130*, 3007–3014.
13. Kibar, Z., Capra, V., and Gros, P. (2007) Toward understanding the genetic basis of neural tube defects. *Clin. Genet. 71*, 295–310.
14. Montcouquiol, M., Sans, N., Huss, D., Kach, J., Dickman, J. D., Forge, A., Rachel, R. A., Copeland, N. G., Jenkins, N. A., Bogani, D., Murdoch, J., Warchol, M. E., Wenthold, R. J., and Kelley, M. W. (2006) Asymmetric localization of Vangl2 and Fz3 indicate novel mechanisms for planar cell polarity in mammals. *J. Neurosci. 26*, 5265–5275.
15. Chacon-Heszele, M. F., and Chen, P. (2009) Mouse models for dissecting vertebrate planar cell polarity signaling in the inner ear. *Brain Res. 1277*, 130–140.
16. Torban, E., Patenaude, A. M., Leclerc, S., Rakowiecki, S., Gauthier, S., Andelfinger, G., Epstein, D. J., and Gros, P. (2008) Genetic interaction between members of the Vangl family causes neural tube defects in mice. *Proc. Natl. Acad. Sci. U.S.A. 105*, 3449–3454.
17. Torban, E., Kor, C., and Gros, P. (2004) Van Gogh-like2 (Strabismus) and its role in planar cell polarity and convergent extension in vertebrates. *Trends Genet 20*, 570–577.
18. Etheridge, S. L., Ray, S., Li, S., Hamblet, N. S., Lijam, N., Tsang, M., Greer, J., Kardos, N., Wang, J., Sussman, D. J., Chen, P., and Wynshaw-Boris, A. (2008) Murine dishevelled 3 functions in redundant pathways with dishevelled 1 and 2 in normal cardiac outflow tract, cochlea, and neural tube development. *PLoS Genet. 4*, e1000259.
19. Curtin, J. A., Quint, E., Tsipouri, V., Arkell, R. M., Cattanach, B., Copp, A. J., Henderson, D. J., Spurr, N., Stanier, P., Fisher, E. M., Nolan, P. M., Steel, K. P., Brown, S. D., Gray, I. C., and Murdoch, J. N. (2003) Mutation of Celsr1 disrupts planar polarity of inner ear hair cells and causes severe neural tube defects in the mouse. *Curr. Biol. 13*, 1129–1133.
20. Wang, Y., and Nathans, J. (2007) Tissue/planar cell polarity in vertebrates: new insights and new questions. *Development 134*, 647–658.
21. Keller, R. (2002) Shaping the vertebrate body plan by polarized embryonic cell movements. *Science 298*, 1950–1954.
22. Wallingford, J. B., Fraser, S. E., and Harland, R. M. (2002) Convergent extension: the molecular control of polarized cell movement during embryonic development. *Dev. Cell 2*, 695–706.
23. Wang, J., Hamblet, N. S., Mark, S., Dickinson, M. E., Brinkman, B. C., Segil, N., Fraser, S. E., Chen, P., Wallingford, J. B., and

Wynshaw-Boris, A. (2006) Dishevelled genes mediate a conserved mammalian PCP pathway to regulate convergent extension during neurulation. *Development 133*, 1767–1778.
24. Wang, Y., Guo, N., and Nathans, J. (2006) The role of frizzled3 and frizzled6 in neural tube closure and in the planar polarity of inner-ear sensory hair cells. *J. Neurosci. 26*, 2147–2156.
25. Torban, E., Wang, H. J., Patenaude, A. M., Riccomagno, M., Daniels, E., Epstein, D., and Gros, P. (2007) Tissue, cellular and sub-cellular localization of the Vangl2 protein during embryonic development: effect of the Lp mutation. *Gene Expression Patterns 7*, 346–354.
26. Reynolds, A., McDearmid, J. R., Lachance, S., De Marco, P., Merello, E., Capra, V., Gros, P., Drapeau, P., and Kibar, Z. (2010) VANGL1 rare variants associated with neural tube defects affect convergent extension in zebrafish. *Mech. Dev. 127*, 385–392.
27. Gravel, M., Iliescu, A., Horth, C., Apuzzo, S., and Gros, P. (2010) Molecular and cellular mechanisms underlying neural tube defects in the loop-tail mutant mouse. *Biochemistry 49*, 3445–3455.
28. Czachorowski, M., Lam-Yuk-Tseung, S., Cellier, M., and Gros, P. (2009) Transmembrane topology of the mammalian Slc11a2 iron transporter. *Biochemistry 48*, 8422–8434.
29. Ellgaard, L., and Helenius, A. (2003) Quality control in the endoplasmic reticulum. *Nat. Rev. Mol. Cell. Biol. 4*, 181–191.
30. Song, H., Hu, J., Chen, W., Elliott, G., Andre, P., Gao, B., and Yang, Y. (2010) Planar cell polarity breaks bilateral symmetry by controlling ciliary positioning, *Nature* (in press).
31. Jessen, J. R., and Solnica-Krezel, L. (2004) Identification and developmental expression pattern of Van Gogh-like 1, a second zebrafish strabismus homologue. *Gene Expression Patterns 4*, 339–344.
32. Torban, E., Wang, H. J., Groulx, N., and Gros, P. (2004) Independent mutations in mouse Vangl2 that cause neural tube defects in looptail mice impair interaction with members of the dishevelled family. *J. Biol. Chem. 279*, 52703–52713.
33. Merte, J., Jensen, D., Wright, K., Sarsfield, S., Wang, Y., Schekman, R., and Ginty, D. D. (2010) Sec24b selectively sorts Vangl2 to regulate planar cell polarity during neural tube closure. *Nat. Cell Biol. 12*, 41–46 (sup pp 41−48).
34. Wansleeben, C., Feitsma, H., Montcouquiol, M., Kroon, C., Cuppen, E., and Meijlink, F. (2010) Planar cell polarity defects and defective Vangl2 trafficking in mutants for the COPII gene Sec24b. *Development 137*, 1067–1073.